Talanta 204 (2019) 224–228

Contents lists available at ScienceDirect

Talanta

journal homepage: www.elsevier.com/locate/talanta

Fabrication of a covalent organic framework and its gold nanoparticle hybrids as stable mimetic peroxidase for sensitive and selective colorimetric detection of mercury in water samples

Wei Li[a], Yang Li[a], Hai-Long Qian[b], Xu Zhao[b], Cheng-Xiong Yang[a], Xiu-Ping Yan[b,*]

[a] College of Chemistry, Research Center for Analytical Sciences, Tianjin Key Laboratory of Molecular Recognition and Biosensing, Nankai University, 94 Weijin Road, Tianjin, 300071, China

[b] State Key Laboratory of Food Science and Technology (Jiangnan University), International Joint Laboratory on Food Safety, Institute of Analytical Food Safety, School of Food Science and Technology, Jiangnan University, Wuxi, 214122, China

ARTICLE INFO

Keywords:
Colorimetric detection
Covalent organic frameworks
AuNPs
Hg^{2+}
Mimetic peroxidase

ABSTRACT

Gold nanoparticles (AuNPs) without surface capping agents are easily aggregated owing to their high surface energy, leading to an unexpected decrease of their catalytic activity. Herein, we report gold nanoparticles decorated covalent organic framework (COF) as mimetic peroxidase for colorimetric detection of mercury. 1,3,5-Tris-(4-formyl-phenyl)triazine (PT) and 4, 4′-azodianiline (Azo) was employed as the monomers to prepare a novel imine based COF PTAzo under solvothermal conditions. AuNPs are further decorated into the PTAzo to form COF-AuNPs hybrid via a citrate reducing method. The COF-AuNPs show high stability, and exhibits enhanced peroxidase mimetic activity in the presence of Hg^{2+}. The Hg^{2+} concentration dependent peroxidase mimetic activity of COF-AuNPs enables the development of a sensitive and selective method for detection of Hg^{2+} in aqueous solution. The developed method gives good linearity in the range of 5–300 nM with the limit of detection of 0.75 nM. The results show that Hg^{2+}-enhanced peroxidase mimetic activity of COF-AuNPs offers great potential for the detection of Hg^{2+} in real samples.

1. Introduction

Gold nanoparticles (AuNPs) have attracted immense interest due to their excellent catalytic activity [1–3]. The catalytic performance of AuNPs highly depends on their dispersibility and accessibility [4]. However, AuNPs without surface capping agents are easily aggregated owing to their high surface energy, leading to an unexpected decrease of their catalytic activity [5,6]. Therefore, a method that prevents AuNPs from aggregation while keeps their intrinsic catalytic activity is highly desirable.

Covalent organic frameworks (COFs) are porous crystalline materials orderly linked by organic monomers [7–9]. Owing to their unique properties and structures, such as large surface area, predicable structures and low density, COFs have shown high potential for applications in diverse fields such as sensing [10–12], catalysis [13,14] and separation [15]. Mercury ion (Hg^{2+}) is a toxic heavy-metal pollutant in the environment. It can cause serious damage to humans and animals even at ppm levels of mercury accumulation [16]. To date, COFs-based approach has been developed for the detection of Hg^{2+} [11]. However, the selectivity and sensitivity of the aforementioned approach was limited due to the lack of specific recognition group and turn-off detection. Thus, a sensitive and selective COFs-based sensor for detection of Hg^{2+} is highly desired.

Integrating COFs with functional nanoparticles is an attractive way to enhance their performance such as solubility and broaden their applications [17–22]. COFs provide rich metal binding sites due to the large surface area and the pre-designable pore size to allow rapid diffusion of substrate molecules [23]. The π electronic architecture is helpful to the absorption of substrate molecules [24,25]. Moreover, COFs can improve the thermal and chemical stability of AuNPs [17].

Herein, we report a one-step reducing method to prepare a highly stable COF supported AuNPs hybrids (COF-AuNPs) for colorimetric detection of Hg^{2+}. A stable, crystalline and porous imine based COF PTAzo was synthesized from monomers 1,3,5-tris-(4-formyl-phenyl) triazine (PT) and 4, 4′-azodianiline (Azo) as an example. The COF-AuNPs show higher stable peroxidase mimetic activity than bare AuNPs. Hg^{2+}-enhanced peroxidase mimetic activity of COF-AuNPs enables efficient oxidation of 3,3′,5,5′-tetramethylbenzidine (TMB) in

* Corresponding author.
E-mail address: xpyan@jiangnan.edu.cn (X.-P. Yan).

https://doi.org/10.1016/j.talanta.2019.05.086
Received 1 April 2019; Received in revised form 10 May 2019; Accepted 20 May 2019
Available online 24 May 2019
0039-9140/

the presence of H_2O_2 for sensitive and selective detection of Hg^{2+}.

2. Experimental section

2.1. Reagents

All chemicals and reagents used are at least of analytical grade. Ultrapure water was purchased from Wahaha Foods Co. (Hangzhou, China). Azo, TMB, $Hg(NO_3)_2$, KNO_3, $Mg(NO_3)_2$, $HAuCl_4$ and sodium citrate were obtained from Sigma-Aldrich Co. LLC (St. Louis, MO, USA). 1,3,5-tris-(4-formyl-phenyl)triazine (PT) was obtained from Chengdu Tongchuangyuan Pharmaceutical Technology Co. (Chengdu, China). o-Dichlorobenzene (o-DCB), N,N-dimethylacetamide (DMAc), N,N-dimethylformamide (DMF) and dichloromethane were purchased from Concord Fine Chemical Research Institute (Tianjin, China).

2.2. Instrumentation

Powder X-ray diffraction (PXRD) patterns were recorded on a D2 PHASER diffractometer (Bruker, German). ^{13}C cross-polarization magic angle spinning solid-state nuclear magnetic resonance (CP-MAS SNMR) experiment was performed on Infinityplus 400 (Varian, USA). Scanning electron microscopy (SEM) image was recorded on an S-3500 N scanning electron microscope (Hitachi, Japan). Transmission electron microscopy (TEM) images were obtained on a JEM-2100 transmission electron microscope (JEOL, Japan) with an accelerating voltage of 200 kV. The Fourier transform infrared (FT-IR) spectra were measured on a Nicolet IR IS10 spectrometer (Nicolet, USA). N_2 adsorption experiment was performed on AutosorbiQ (Quantachrome, USA) at 77 K. The pore size distribution of prepared COFs was calculated using the density functional theory model. UV–Vis absorption spectra were recorded at room temperature on a UV-3600plus spectrophotometer (Shimadzu, Japan). Absorbance of the oxidized TMB (oxTMB) at 652 nm was monitored for quantitative analysis.

2.3. Synthesis of PTAzo and COF-AuNPs

PT (39.3 mg, 0.1 mmol), Azo (31.8 mg, 0.15 mmol), 1.5 mL of o-DCB and 1.5 mL of DCM were mixed in a Schlenk tube, flash frozen at 77 K (liquid N_2 bath) and degassed by three freeze-pump-thaw cycles. Then, the tube was sealed off and heated at 120 °C for 3 days. The precipitate was collected by centrifugation and washed with DMF thrice and dichloromethane twice. The collected powder was dried in vacuum overnight to get PTAzo in ca. 79% isolated yield.

PTAzo (7.5 mg) was added into the $HAuCl_4$ solution (10 mL, 1 mM) and stirred for 5 min. Then, sodium citrate aqueous solution (400 μL, 100 mM) was added to the mixture. After 30 min reaction, the mixture was centrifuged at 6000 rpm for 5 min. The precipitates were washed with ultrapure water three times. Finally, the obtained COF-AuNPs precipitates were collected and diluted to 1500 mg L^{-1} with ultrapure water for further use.

2.4. Colorimetric detection of Hg^{2+}

Tap water and lake water samples were collected locally. Waste water was collected from an industrial area in Wuxi. Tap water, lake water and waste water samples were filtered through 0.22 μm micropore films before use. Water samples (100 μL) were mixed with acetic acid solution (900 μL, pH 4.0) and a slight shaking for further measurement. COF-AuNPs (20 μL, 1500 mg L^{-1}), H_2O_2 (40 μL, 5 M), TMB (20 μL, 30 mM) and Hg^{2+} standard solution (20 μL) or the prepared water solution (20 μL) was added into acetic acid solution (100 μL, pH 4.0) and incubated at 35 °C for 10 min before measurements. Then, the absorbance of the solution at 652 nm was measured for quantitative analysis.

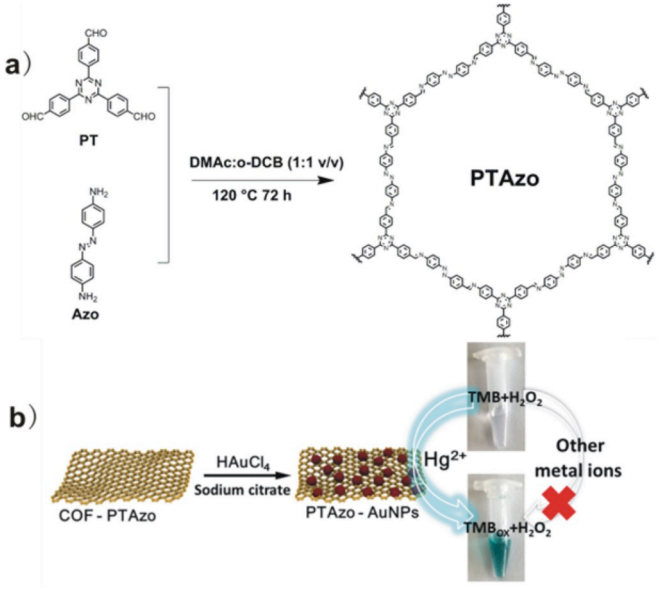

Fig. 1. (a) Illustration of the synthesis of PTAzo; (b) Scheme for the construction of COF-AuNPs for colorimetric detection of Hg^{2+}.

3. Results and discussion

3.1. Preparation and characterization of PTAzo

PTAzo was prepared from PT and Azo in a mixture of o-DCB and DMAc under solvothermal conditions (Fig. 1a). The monomer PT possesses planar structure that guarantees high crystalline stability and easy synthesis of PTAzo [26]. PTAzo contains triazine and N element to facilitate the formation of AuNPs. Such structures and properties make PTAzo an ideal platform for loading AuNPs.

PXRD pattern shows several peaks at 2.27°, 4.25°, 5.87° and 25.71°, being consistent with the simulated pattern for PTAzo (Fig. 2a; Fig. S1-S2 and Table S1) produced with eclipsed AA stacking mode (a = b = 48.3036 Å, c = 3.4748 Å, α = β = 90° and γ = 120°). FT-IR spectrum of PTAzo shows a sharp peak at 1667 cm^{-1} for the C═N stretching. The concomitant absence of the N-H stretching vibration (3471 and 3378 cm^{-1}) and the decrease of the C═O stretching vibration (1702 cm^{-1}) indicates the condensation reaction between the aldehyde group of PT and the amine group of Azo (Fig. 2b). The peak at 163 ppm in ^{13}C CP-MAS SNMR spectra also confirms the successful construction of imine bonds (Fig. 2c). All the above results demonstrate that PTAzo was successfully prepared.

The morphology, stability and permanent porosity of PTAzo were further characterized. Both TEM and SEM images show the obvious sheet structure of PTAzo due to the strong π-π stacking interaction between adjacent layers (Fig. 2d and Fig. S3). Thermogravimetric analysis shows the high thermal stability (up to 400 °C) of PTAzo (Fig. S4a). PXRD patterns show PTAzo was also stable in acid, alkaline solution and various organic solvents (Fig. S4b). PTAzo possesses BET surface area of 221 $m^2 g^{-1}$ (Fig. S5a) mainly with a mesoporous pore size of ca. 43 Å (Fig. S5b). Such large pore-size is helpful for the diffusion of substrate molecules and the accommodation of AuNPs [23,27].

3.2. Preparation and characterization of the COF-AuNPs

COF-AuNPs was further prepared by adding sodium citrate into a mixture of $HAuCl_4$ and PTAzo under vigorous stirring (Fig. 1b). The PXRD pattern and FT-IR spectrum of COF-AuNPs suggested the structural regularity and chemical composition of COF remained intact (Fig. 3a; 3b). The additional peak of PXRD pattern at 38.2° and 44.3°

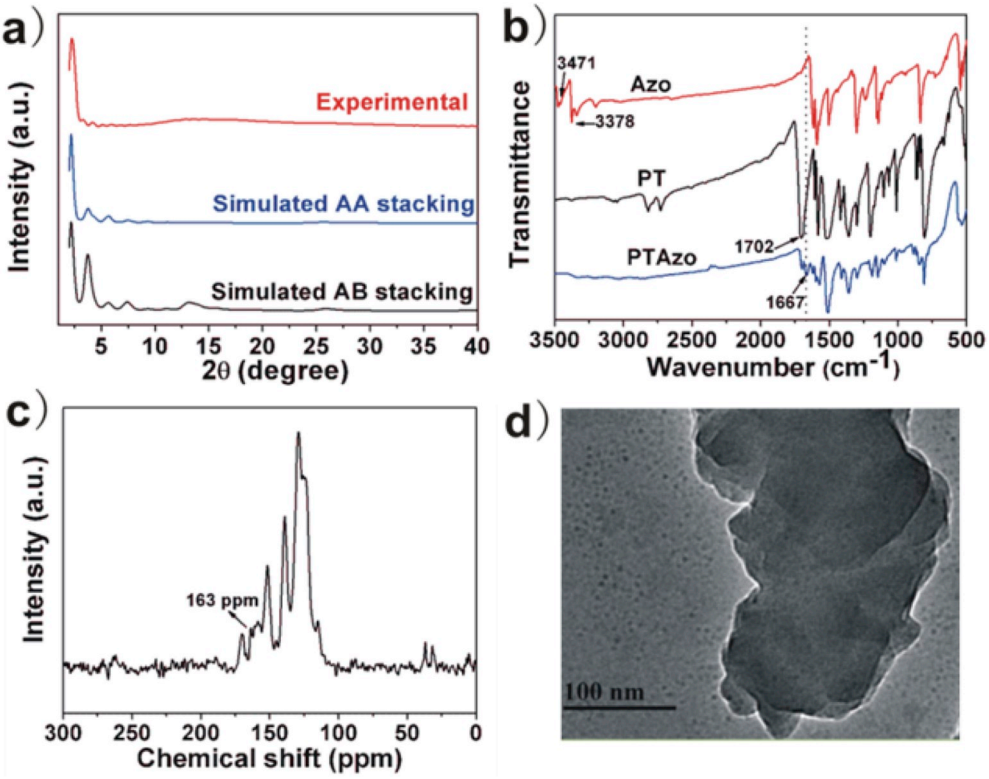

Fig. 2. (a) Experimental and simulated PXRD patterns of PTAzo. (b) FT-IR spectra of Azo, PT and PTAzo. (c) ^{13}C CP-MAS SNMR spectra of PTAzo. (d) TEM image of PTAzo.

confirmed the successful incorporation of AuNPs into the COF. The TEM image and the change of zeta potential also demonstrated the formation of COF-AuNPs hybrid (Fig. 3c and d). The reduction of Au^{3+} to Au^0 was proved by X-ray photoelectron spectroscopy (XPS) analysis. The XPS spectra of COF-AuNPs in the 4f region show typical peaks at 85.1 eV ($4f_{5/2}$) and 81.5 eV ($4f_{7/2}$) for Au^0. The XPS spectra of COF-AuNPs also suggest the presence of partial Au^{3+} and Au^{+} on the surface of AuNPs (Fig. S6) [28].

3.3. Hg^{2+}-enhanced peroxidase mimetic activity of COF-AuNPs

The effect of Hg^{2+} on the peroxidase-like activity of COF-AuNPs

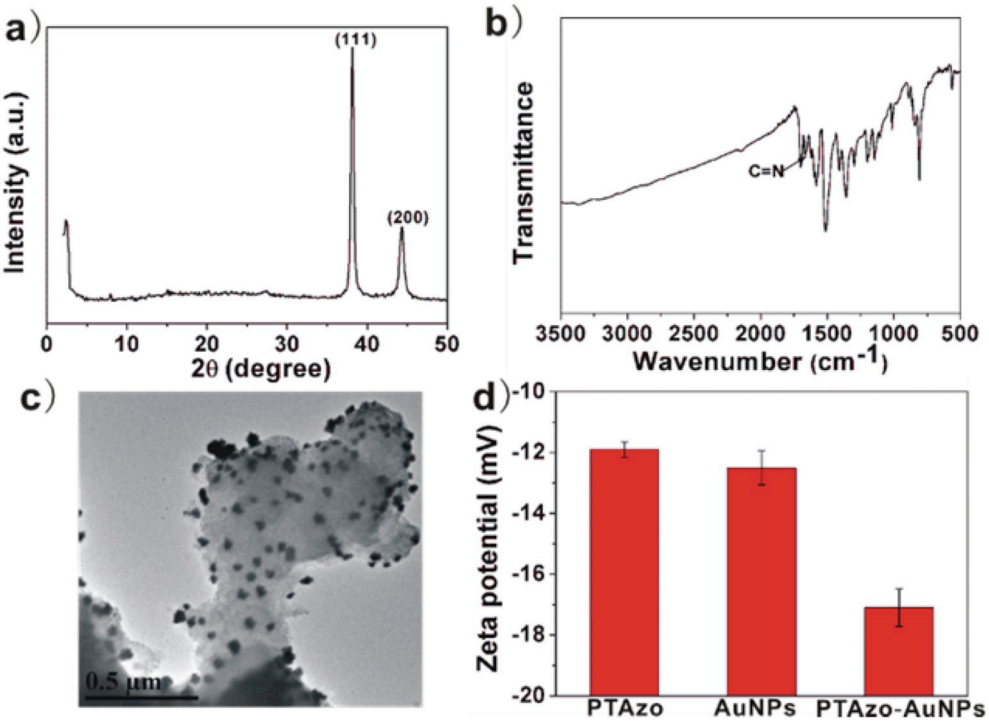

Fig. 3. (a) PXRD pattern of COF-AuNPs. (b) FT-IR spectrum of COF-AuNPs. (c) TEM image of COF-AuNPs. (d) Zeta potential of PTAzo, AuNPs and COF-AuNPs.

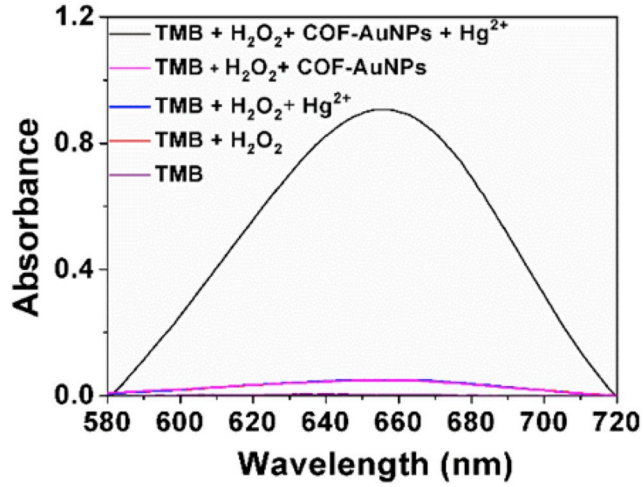

Fig. 4. Absorption spectra of TMB, H_2O_2 + TMB, Hg^{2+} + TMB + H_2O_2, COF-AuNPs + H_2O_2 + TMB and Hg^{2+} + COF-AuNPs + TMB + H_2O_2.

was examined. It was reported that Hg^{2+} was reduced to Hg^0 by citrate sodium and deposited on the surface of AuNPs, improving the peroxidase-like activity of AuNPs [29]. Here, we also found that Hg^{2+} enhanced the peroxidase-like activity of COF-AuNPs in the reaction of TMB and H_2O_2. TMB, H_2O_2 + TMB, Hg^{2+} + H_2O_2 + TMB or COF-AuNPs + TMB + H_2O_2 gave no obvious absorption peaks from 580 to 720 nm (Fig. 4). In contrast, addition of Hg^{2+} to the mixture of TMB, H_2O_2 and COF-AuNPs led to a strong absorption peak at 652 nm, indicating that Hg^{2+} can stimulate the peroxidase-like activity of COF-AuNPs. It should be noted that addition of Hg^{2+} to the mixture of H_2O_2 and TMB did not result in obvious absorption peaks from 580 to 720 nm, suggesting that COF-AuNPs also play an important role in colour reaction.

COF-AuNPs is more water soluble than COF and more stable than AuNPs prepared via sodium citrate reducing method (Fig. S7a, 7b) [29,30]. AuNPs also showed peroxidase-like activity in the presence of Hg^{2+}, H_2O_2 and TMB [29], but was easily aggregated and lose the peroxidase-like activity in the presence of NaCl (50 mM) (Fig. S8a). The absorbance of aggregated AuNPs at 600–700 nm may affect the absorbance of TMB (652 nm). In contrast, the peroxidase-like activity of COF-AuNPs remained good in the presence of 50 mM NaCl (Fig. S8b). The above results suggest that COF-AuNPs was much more stable than AuNPs as a mimic peroxidase for colorimetric detection.

3.4. Analytical performance of COF-AuNPs for detection of Hg^{2+}

To achieve the best performance of the peroxidase-like activity of COF-AuNPs, the effects of pH, temperature, reaction time, H_2O_2, COF-AuNPs and TMB concentration were investigated (Fig. S9). The results show that the optimal pH, temperature, reaction time, the concentration of H_2O_2, COF-AuNPs and TMB were 4.0, 35 °C, 10 min, 1 M, 150 mg L^{-1} and 3 mM, respectively. Under the best performance of peroxidase-like activity of COF-AuNPs, the absorbance of the mixture solution of COF-AuNPs + TMB + H_2O_2 heavily depended on the Hg^{2+} concentration (Fig. 5a), which was also observed with the naked eye (Fig. 5b). The enhanced absorbance (ΔA) increased linearly as the concentration of Hg^{2+} (C, nM) increased from 5 to 300 nM with a calibration function of $\Delta A = 0.0028C + 0.0024$ and a coefficient of determination (R^2) of 0.9973 (Fig. 5c). The limit of detection (LOD, 3s) for Hg^{2+} is 0.75 nM, much lower than the maximum level of Hg^{2+} in drinking water (10 nM) permitted by the U.S. Environmental Protection Agency. The LOD of the developed method is comparable to or lower than those of previous methods for the detection of Hg^{2+} (Table S2).

3.5. Selectivity of COF-AuNPs for detection of Hg^{2+}

To reveal the selectivity of the developed method, the effect of 10-fold (3 μM) of other metal ions (Ca^{2+}, Mn^{2+}, Cr^{3+}, Pb^{2+}, Ba^{2+}, K^+, Na^+, Fe^{3+}, Mg^{2+} and Cu^{2+}) on the determination of Hg^{2+} (0.3 μM) were examined. The results indicate that the coexistence of these interfering substances had little effect on the detection of Hg^{2+} (Fig. 5d). The high selectivity for Hg^{2+} originated from the high affinity of Hg^0 to Au^0 on the surface of COFs-AuNPs [29]. The precision for eleven

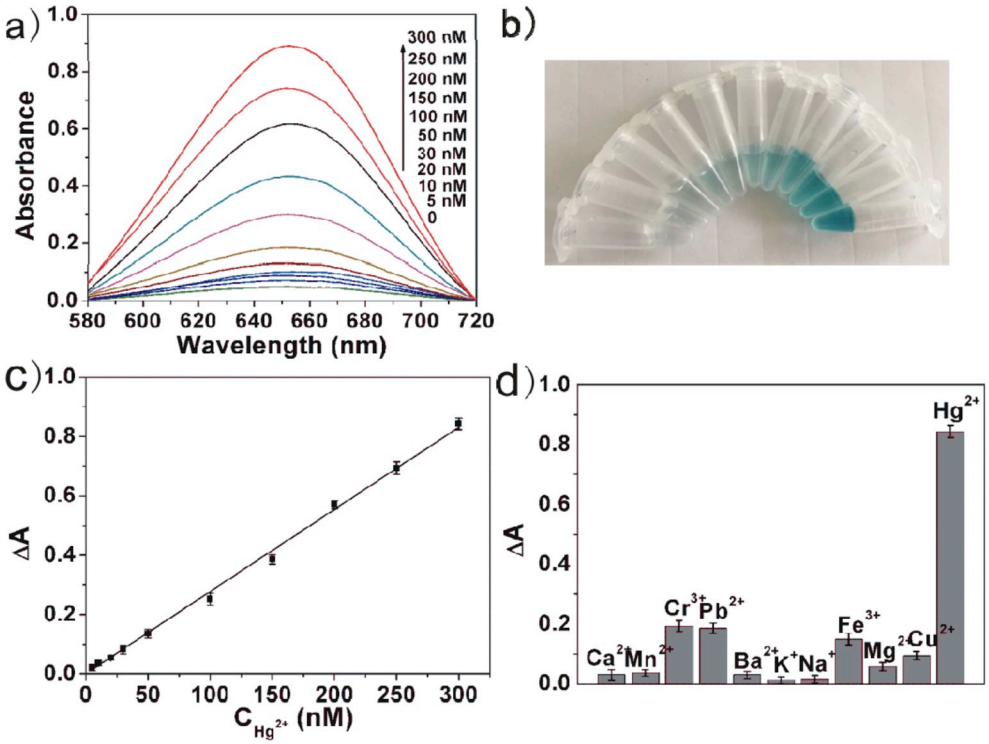

Fig. 5. (a) Effect of Hg^{2+} concentration on the absorption spectra of TMB in the presence of COF-AuNPs and H_2O_2. (b) Corresponding solution colour change of (a). (c) Plot of the change of absorbance (ΔA) against Hg^{2+} concentration. (d) Peroxidase-like performance of COF-AuNPs for the detection of Hg^{2+} (0.3 μM) in the presence of various metal ions (3 μM). The error bar represents the standard deviation of triplicate measurements. (For interpretation of the references to color in this figure legend, the reader is referred to the Web version of this article.)

Table 1
Analytical results for the determination of Hg^{2+} in water samples.

Samples	Spiked Hg^{2+}/nM	Concentration found (mean ± s, n = 3)/nM
Tap water	0	Not detected
	10 nM	9.9 ± 0.7
	30 nM	29.4 ± 1.5
	80 nM	78.2 ± 2.3
Lake	0	Not detected
	10 nM	10.1 ± 0.9
	30 nM	29.5 ± 1.3
	80 nM	82.4 ± 2.5
Waster water	0	17.2 ± 1.1
	10 nM	28.2 ± 1.3
	30 nM	45.9 ± 2.5
	80 nM	97.6 ± 2.4

replicate measurements of 50 nM Hg^{2+} was 2.8% (relative standard deviation, RSD). The robustness of the developed method was tested by intra-day and inter-day study. The RSDs for intra-day (n = 4) and inter-day (n = 3) study are 3.1% and 4.3%, respectively.

The developed method was applied to the determination of Hg^{2+} in GBW(E)080393 (Certified Reference Material for Hg in simulated natural water) to evaluate the accuracy. The samples were diluted 1000 times to ensure that the Hg^{2+} content is in the linear range. The determined concentration of Hg^{2+} (0.095 ± 0.004 mg L^{-1}, $n = 5$) agreed well with the certified value (0.100 ± 0.004 mg L^{-1}). The proposed method was further applied to the determination of Hg^{2+} in tap water, lake water and waste water. The quantitative spike recoveries for the detection of Hg^{2+} in water samples ranged from 97% to 104% (Table 1), suggesting that the developed method has a great potential for Hg^{2+} assay in real samples.

4. Conclusions

In summary, we have reported a novel imine COF PTAzo and its AuNPs hybrid (COF-AuNPs) via one-step reducing method. The COF enhanced the stability while kept intrinsic catalytic activity of AuNPs. Based on Hg^{2+}-enhanced peroxidase mimetic activity, COF-AuNPs show promising application in sensitive and selective detection of Hg^{2+} in real samples.

Notes

The authors declare no competing financial interest.

Acknowledgements

This work was supported by National Natural Science Foundation of China (Grant 21775056), the China Postdoctoral Science Foundation (Grants 2018M630511, 2018M630510), the National First-class Discipline Program of Food Science and Technology (Grant JUFSTR20180301), and the Fundamental Research Funds for the Central Universities (Grant JUSRP51714B).

Appendix A. Supplementary data

Supplementary data to this article can be found online at https://doi.org/10.1016/j.talanta.2019.05.086.

References

[1] C. Della Pina, E. Falletta, L. Prati, M. Rossi, Selective oxidation using gold, Chem. Soc. Rev. 37 (2008) 2077–2095.
[2] Z.-Y. Zhou, N. Tian, J.-T. Li, I. Broadwell, S.-G. Sun, Nanomaterials of high surface energy with exceptional properties in catalysis and energy storage, Chem. Soc. Rev. 40 (2011) 4167–4185.
[3] H. Wei, E.k. Wang, Nanomaterials with enzyme-like characteristics (nanozymes): next-generation artificial enzymes, Chem. Soc. Rev. 42 (2013) 6060–6093.
[4] K.X. Cui, W.F. Zhong, L.L. Li, Z.Y. Zhuang, L.Y. Li, J.H. Bi, Y. Yu, Well-defined metal nanoparticles@covalent organic framework yolk–shell nanocages by ZIF-8 template as catalytic nanoreactors, Small 15 (2019) 1804419.
[5] R.J. White, R. Luque, V.L. Budarin, J.H. Clark, D.J. Macquarrie, Supported metal nanoparticles on porous materials: methods and applications, Chem. Soc. Rev. 38 (2009) 481–494.
[6] Y. Jv, B.X. Li, R. Cao, Positively-charged gold nanoparticles as peroxidase mimic and their application in hydrogen peroxide and glucose detection, Chem. Commun. 46 (2010) 8017–8019.
[7] A.P. Côté, A.I. Benin, N.W. Ockwig, M. O'Keeffe, A.J. Matzger, O.M. Yaghi, Porous, crystalline, covalent organic frameworks, Science 310 (2005) 1166–1170.
[8] X. Feng, X.S. Ding, D.L. Jiang, Covalent organic frameworks, Chem. Soc. Rev. 41 (2012) 6010–6022.
[9] A.G. Slater, A.I. Cooper, Function-led design of new porous materials, Science 348 (2015) aaa8075.
[10] G. Das, B.P. Biswal, S. Kandambeth, V. Venkatesh, G. Kaur, M. Addicoat, T. Heine, S. Verma, R. Banerjee, Chemical sensing in two dimensional porous covalent organic nanosheets, Chem. Sci. 6 (2015) 3931–3939.
[11] S.-Y. Ding, M. Dong, Y.-W. Wang, Y.-T. Chen, H.-Z. Wang, C.-Y. Su, W. Wang, Thioether-based fluorescent covalent organic framework for selective detection and facile removal of mercury(II), J. Am. Chem. Soc. 138 (2016) 3031–3037.
[12] Z.P. Li, Y.W. Zhang, H. Xia, Y. Mu, X.M. Liu, A robust and luminescent covalent organic framework as a highly sensitive and selective sensor for the detection of Cu^{2+} ions, Chem. Commun. 52 (2016) 6613–6616.
[13] S.-Y. Ding, J. Gao, Q. Wang, Y. Zhang, W.-G. Song, C.-Y. Su, W. Wang, Construction of covalent organic framework for catalysis: Pd/COF-LZU1 in Suzuki-Miyaura coupling reaction, J. Am. Chem. Soc. 133 (2011) 19816–19822.
[14] X. Han, Q.C. Xia, J.J. Huang, Y. Liu, C.X. Tan, Y. Cui, Chiral covalent organic frameworks with high chemical stability for heterogeneous asymmetric catalysis, J. Am. Chem. Soc. 139 (2017) 8693–8697.
[15] H.-L. Qian, C.-X. Yang, W.-L. Wang, C. Yang, X.-P. Yan, Advances in covalent organic frameworks in separation science, J. Chromatogr. A 1542 (2018) 1–18.
[16] L.Y. Chen, S.J. Park, D. Wu, H.M. Kim, J. Yoon, A two-photon fluorescent probe for colorimetric and ratiometric monitoring of mercury in live cells and tissues, Chem. Commun. 55 (2019) 1766–1769.
[17] P. Pachfule, S. Kandambeth, D. Diaz Diaz, R. Banerjee, Highly stable covalent organic framework-Au nanoparticles hybrids for enhanced activity for nitrophenol reduction, Chem. Commun. 50 (2014) 3169–3172.
[18] L. Stegbauer, K. Schwinghammer, B.V. Lotsch, A hydrazone-based covalent organic framework for photocatalytic hydrogen production, Chem. Sci. 5 (2014) 2789–2793.
[19] X.F. Shi, Y.J. Yao, Y.L. Xu, K. Liu, G.S. Zhu, L.F. Chi, G. Lu, Imparting catalytic activity to a covalent organic framework material by nanoparticle encapsulation, ACS Appl. Mater. Interfaces 9 (2017) 7481–7488.
[20] Y. Li, C.-X. Yang, X.-P. Yan, Controllable preparation of core-shell magnetic covalent-organic framework nanospheres for efficient adsorption and removal of bisphenols in aqueous solution, Chem. Commun. 53 (2017) 2511–2514.
[21] H.-L. Qian, C. Yang, X.-P. Yan, Layer-by-layer preparation of 3D covalent organic framework/silica composites for chromatographic separation of position isomers, Chem. Commun. 54 (2018) 11765–11768.
[22] G.-J. Chen, X.-B. Li, C.-C. Zhao, H.-C. Ma, J.-L. Kan, Y.-B. Xin, C.-X. Chen, Y.-B. Dong, Ru nanoparticles-loaded covalent organic framework for solvent-free one-pot tandem reactions in air, Inorg. Chem. 57 (2018) 2678–2685.
[23] Y.H. Xiong, Y.M. Qin, L.J. Su, F.G. Ye, Bioinspired synthesis of Cu^{2+}-modified covalent triazine framework: a new highly efficient and promising peroxidase mimic, Chem. Eur J. 23 (2017) 11037–11045.
[24] Y.W. Peng, Y. Huang, Y.H. Zhu, B. Chen, L.Y. Wang, Z.C. Lai, Z.C. Zhang, M.T. Zhao, C.L. Tan, N.L. Yang, F.W. Shao, Y. Han, H. Zhang, Ultrathin two-dimensional covalent organic framework nanosheets: preparation and application in highly sensitive and selective DNA detection, J. Am. Chem. Soc. 139 (2017) 8698–8704.
[25] P.-F. Wei, M.-Z. Qi, Z.-P. Wang, S.-Y. Ding, W. Yu, Q. Liu, L.-K. Wang, H.-Z. Wang, W.-K. An, W. Wang, Benzoxazole-linked ultrastable covalent organic frameworks for photocatalysis, J. Am. Chem. Soc. 140 (2018) 4623–4631.
[26] A. Halder, S. Kandambeth, B.P. Biswal, G. Kaur, N.C. Roy, M. Addicoat, J.K. Salunke, S. Banerjee, K. Vanka, T. Heine, S. Verma, R. Banerjee, Decoding the morphological diversity in two dimensional crystalline porous polymers by core planarity modulation, Angew. Chem. Int. Ed. 55 (2016) 7806–7810.
[27] S.-Y. Ding, W. Wang, Covalent organic frameworks (COFs): from design to applications, Chem. Soc. Rev. 42 (2013) 548–568.
[28] H. Al-Johani, E. Abou-Hamad, A. Jedidi, C.M. Widdifield, J. Viger-Gravel, S.S. Sangaru, D. Gajan, D.H. Anjum, S. Ould-Chikh, M.N. Hedhili, A. Gurinov, M.J. Kelly, M. El Eter, L. Cavallo, L. Emsley, J.-M. Basset, The structure and binding mode of citrate in the stabilization of gold nanoparticles, Nat. Chem. 9 (2017) 890–895.
[29] Y.J. Long, Y.F. Li, Y. Liu, J.J. Zheng, J. Tang, C.Z. Huang, Visual observation of the mercury-stimulated peroxidase mimetic activity of gold nanoparticles, Chem. Commun. 47 (2011) 11939–11941.
[30] G.K. Darbha, A.K. Singh, U.S. Rai, E. Yu, H. Yu, P. Chandra Ray, Selective detection of mercury (II) ion using nonlinear optical properties of gold nanoparticles, J. Am. Chem. Soc. 130 (2008) 8038–8043.